Associated aspects on structure, morphology and photoluminescence of $MgAl_2O_4$:x% Gd^{3+} nanophosphor prepared via citrate sol-gel method

Setumo Victor Motloung[1,2*], Tshwafo Ellias Motaung[3], Thulani Thokozani Hlatshwayo[4], Lehlohonolo Fortune Koao[5], Thembinkosi Donald Malevu[6], Siyasanga Mpelane[7]

[1]Department of Physics, Nelson Mandela University, P. O. Box 77000, Port Elizabeth 6031, South Africa

[2]Department of Physics, Sefako Makgatho Health Sciences University, P.O. Box 94, Medunsa, 0204, South Africa

[3]Department of Chemistry, University of Zululand, KwaDlangezwa, 3886, South Africa

[4]Department of Physics, University of Pretoria, Pretoria, 0002, South Africa

[5]Department of Physics, University of the Free State (Qwaqwa Campus), Private Bag X13, Phuthaditjhaba, 9866, South Africa

[6]School of Chemistry and Physics, Westville Campus, University of KwaZulu-Natal, Private Bag X54001, Durban 4000, South Africa

[7]Department of Chemistry, University of Johannesburg, P.O. Box: 524, Auckland Park, 2006, South Africa

Corresponding author:

E-mail: cchataa@gmail.com (Setumo Victor Motloung)

Abstract

$MgAl_2O_4$:x% Gd^{3+} ($0 \leq x \leq 3$) nano-powders were prepared via citrate sol-gel method. The X-ray diffraction (XRD) confirmed that the prepared samples consists of the cubic crystalline structures. There was no secondary phases due to Gd^{3+} doping. The estimated average grain sizes were found to be in the order of 8 nm. Energy dispersive spectroscopy (EDS) showed the presence of the anticipated elements (Mg, Al, O, and Gd). The scanning electron microscope (SEM) results revealed that the morphology of the samples is influenced by the Gd^{3+} concentration. Transmission electron microscopy (TEM) analysis revealed that the prepared samples are in the nano-scale range. Selected area electron diffraction (SAED)

patterns indicated highly crystalline structure and the intensities of the bright spots varied with Gd^{3+} concentration. Photoluminescence (PL) studies showed two distinct emission peaks at 385 and 392 nm, which are certainly attributed to the defects levels located at different positions on the host material ($MgAl_2O_4$). The emission peaks located at 315 and 628 nm were respectively attributed to the $^6P_{7/2} \rightarrow {}^8S_{7/2}$ and $^6G_{7/2} \rightarrow {}^6P_{3/2}$ transitions in Gd^{3+} ion. The luminescence intensity of the 388 nm decreased with an increase in the Gd^{3+} concentration. Commision Internationale de l'Eclairage (CIE) coordinates showed that the violet emission color from host cannot be tuned by varying Gd^{3+} concentration.

Keywords $MgAl_2O_4$, Sol-gel, Nanocrystal, Gd^{3+} doping, Luminescence, CIE

1. Introduction

Recently, many aluminate materials have been extensively studied as phosphors for the next generation of display and lighting devices.[1] Magnesium aluminate ($MgAl_2O_4$) spinel has attracted many researchers around the globe based on the unique combination of optical and mechanical properties both at normal and elevated temperatures.[2] $MgAl_2O_4$ strength in both temperatures is due to the fact that it has no phase transition up to the melting point. As a result, $MgAl_2O_4$ has received great attention as a technologically important material on account of its attractive properties such as high melting point (2135 ^oC), high chemical inertness and high thermal stability.[3] It is widely used in many areas like fusion technology,[4] nanodevices,[5] humidity sensors,[6] photoluminescent material[7] and catalysts for many reactions.[8,9] The need of tuning the optical properties made researchers to intentionally incorporate or dope various types of foreign impurities such as rare earth (RE) metals into $MgAl_2O_4$ (host) crystal structure.[10] RE ions are well known for their high color purity emission lines due to their f-f or f-d transitions.[11] The incorporation of the RE ions such as Eu^{3+}, Tb^{3+} and Gd^{3+} have been reported in literature on different host materials.[11] For the examples, Omkaram et al.[12] reported the emission analysis of green-emitting Tb^{3+} doped $MgAl_2O_4$ phosphors. Khatkar et al.[13] reported the preparation and photoluminescence characteristics of Eu^{3+} doped $MgAl_{1.8}Y_{0.2}O_4$ nanocrystals. Trivalent gadolinium (Gd^{3+}) is one of the most investigated RE ions on various host materials during the past years. It is a well-known quantum cutting or photon cascade emission ion.[11] Quantum cutting (QC) is a phenomenon that one high-energy photon is converted into two or more than two photons with low energy.[14] Gd^{3+} ion has $4f^7$ electronic configuration and the energy gap between the ground state ($^8S_{7/2}$) and the excited state ($^6P_{7/2}$) is 32000 cm^{-1}.[15] Singh et al.[11] reported the synthesis of Gd^{3+} doped $MgAl_2O_4$ using a simple and fast (short time of 5 min) one-step combustion method. The luminescence of the Gd^{3+} doped $MgAl_2O_4$ shows two emission bands centered at 306 nm ($^6P_{5/2} \rightarrow {}^8S_{7/2}$)

and 312 nm ($^6P_{7/2} \rightarrow {}^8S_{7/2}$), under ultraviolet (UV) excitation 273 nm. The narrow ultraviolet burning rays (UVB) peak centered at 312 nm serves the better material for phototherapy lamp preparation.[11] Gd^{3+} ion can also exhibits emission around 628 nm due to $^6G_{7/2} \rightarrow {}^6P_{3/2}$ transitions.[16] From synthesis point of view, variety of techniques such as combustion,[11] sol-gel,[17] spray drying,[18], freeze-drying[19] and mechanical activation[20] have been developed to synthesize $MgAl_2O_4$ phosphor. The advantages of the sol-gel method are; it offers high purity, homogeneity, single phase, small and uniform particles size at relatively lower preparation temperature in comparison with other conventional methods.[17,22] In this work, the citrate sol-gel method was hence adopted as an alternative for the synthesis of $MgAl_2O_4$:x% Gd^{3+} nanophosphors.

Even though $MgAl_2O_4$:Gd^{3+} prepared by combustion method was reported in the literature.[11] The focus was more on the luminescence and electron paramagnetic resonance (EPR) investigation of ultraviolet emitting $MgAl_2O_4$:Gd^{3+} phosphors. In this present work, we report the citrate sol-gel synthesis of the $MgAl_2O_4$:x% Gd^{3+} ($0 \leq x \leq 3$) nanophosphor. This study focuses on the effects of the variation of the concentration of the Gd^{3+} ions on the morphology, structure and photoluminescence properties of the $MgAl_2O_4$:x% Gd^{3+} ($0 \leq x \leq 3$) nanophosphor with the main aim of producing more alternative phosphor materials for the practical applications such as blue light emitting diodes (BLED's) and better material for phototherapy lamp preparation.

2. Experimental

2.1 Sample synthesis

The $MgAl_2O_4$: x% Gd^{3+} ($0 \leq x \leq 3$) powder samples were synthesized using the citrate sol-gel method. Citric acid (CA) was used as a chelating agent. The host ($MgAl_2O_4$) was prepared by dissolving $Mg(NO_3)_2.6H_2O$ (98%), $Al(NO_3)_3.9H_2O$ (98.5%) and CA ($C_8H_8O_7.H_2O$) (99%) in deionized water. $Al(NO_3)_3.9H_2O$ was added to $Mg(NO_3)_2.6H_2O$ to form a homogeneous mixture in which the molar ratio of Mg:Al was 1:2. To this solution, CA in the molar ratio of CA:(Mg^{2+} + Al^{3+}) equals to 1:1 was also added. Gd^{3+} doped samples were prepared by adding different concentrations of the $Gd(NO_3)_3.6H_2O$ (99.9%) in the range of ($0 \leq x \leq 3$) into the separate beakers of the host solution. In all samples, the temperature was kept ~ 80 ^oC while constantly stirring using a magnetic stirrer until the transparent gel solutions of the mixed metals were formed. The prepared gel were annealed at 800 ^oC in a furnace for 1 h. The resulting products were ground using a pestle and mortar and later analyzed using different techniques.

2.2 Sample characterization

The crystal structure of the samples was characterized by X-ray powder diffraction (XRD) (Bruker D8-Advance powder XRD) with Cu Kα (1.5405Å) radiation. In addition, the samples were characterized by Shimadzu Super scan ZU SSX-550 scanning electron microscope (SEM) attached with energy-dispersive X-ray spectroscopy (EDS), transmission electron microscopy (TEM) performed with was performed with a JEOL JEM 2100 containing a LaB_6 filament. The photoluminescence (PL) study was performed at room temperature using Hitachi F-7000 fluorescence spectrophotometer with a 150 W Xenon lamp as an excitation source.

3. Results and discussion

3.1 XRD results

Fig.1 shows the XRD patterns of the $MgAl_2O_4$:x% Gd^{3+} ($0 \leq x \leq 3$) series. The observed diffraction peaks correspond to those of the standard patterns of the cubic $MgAl_2O_4$ (JCPDS 75-1796) structure. No extra diffraction peaks which can be related to the secondary phases were detected suggesting that the prepared powder samples consists of the single phase. The average value of the lattice constant *(a)* of the prepared samples was calculated to be 8.03 Å (see Table I), which is very close to the previously reported value of 8.05 Å.[23] The crystallite size was calculated from (400) diffraction peaks by using Scherrer's equation.[24] The calculated crystallite sizes are presented in Table I. It is clear that doping $MgAl_2O_4$ with various Gd^{3+} concentration does not significantly influence crystallite sizes.

The analysis of the (400) diffraction peak is shown in Fig. 2. Generally and in comparison with the host (un-doped) sample, it can be clearly seen that there is a slightly peak shift to the higher angle at the higher Gd^{3+} concentration. A clear shifting of the (400) diffraction peaks toward higher angle (especially for the x = 1.8 and 2.6%) is attributed to the decrease in *a* as shown in Table 1. Note that the *a* values were calculated by using equation (1)[25,2]:

$$a = d\sqrt{h^2 + l^2 + k^2} \tag{1}$$

where *d* is the crystalline surface distance for *hlk* indices, which is given by equation (2)[27]:

$$d = \frac{\lambda}{2\sin\theta} \tag{2}$$

where is the λ stands for the radiation wavelength (0.15406 nm) and θ is the angle of diffraction.

Based on the ionic radiuses of the Gd^{3+} (0.94 Å),[28] Mg^{2+} (0.72 Å)[23,29] and Al^{3+} (0.53 Å),[23,29,30] it was expected that the shift be towards the lower angle if the Gd^{3+} replaces either Mg^{2+} or Al^{3+}. In $ZnAl_2O_4$:x% Pb^{2+} system, our group[31] have previously reported similar kind of behavior not obeying the Vegard's law. Thus, in this study the decrease in *a* (for the x = 1.8 and 2.6%) is therefore attributed to the shrinkage or suppression of the Gd^{3+} outer electron shell due to its electronic interactions with more neighbouring Mg^{2+} ions, which causes its ionic radius becomes smaller than that one of Mg^{2+} ion and hence the observed decrease in *a* or shift to the lager angle. It is important to note that at the higher Gd^{3+} concentration (e.g. x = 3.0%) the shift is to the lower angle which can be attributed to the increase of the *a*. The proposed reason for this behavior is that; the electronic interaction of the neighboring Mg^{2+} ions becomes insignificant as more Gd^{3+} ions (due to higher concentration) replaces or substitutes Mg^{2+} ions and as a results, the Gd^{3+} outer electron shell can no longer be suppressed anymore. Thus, the system starts to obey the Vegard's law. The other possible reason might be the fact that maybe the Gd^{3+} is no longer replacing the Mg^{2+} but Al^{3+} ions at the higher Gd^{3+} concentration (x = 3.0%). Our group[32] have previously observed similar kind of behavior on the $ZnAl_2O_4$:x% Cr^{3+} system where Cr^{3+} was observed to be able to replace either Zn^{2+} or Al^{3+}. The results clearly demonstrated that the replacement or substitution of Zn^{2+} or Al^{3+} highly depends on the Cr^{3+} concentration, which might also be the case in this results. The change on the (400) diffraction peak intensity indicates that the crystallinity depends on the Gd^{3+} concentration.[33]

3.2 EDS and SEM results

The elementary composition of the prepared nanopowder samples were confirmed by the EDS technique as shown in Fig. 3. In Fig. 3a, EDS results show that the host sample consists of the Mg, Al and O. Fig. 3b and c shows the presence of Gd on the spectra. Although the EDS technique cannot be used to quantify the dopants concentration, it is interesting to observe that the wt% for the x = 1.4% is lower than that of the x = 3% doped sample. The C peak in all of the spectrum in Fig. 3a – c is attributed to carbon (C) tape used during the EDS measurement. The EDS results did not detect any presence of the secondary phases, which agrees pefectly with the XRD results (see Fig. 1).

To confirm the compositional distribution of the constituent elements of the powder samples, the EDS maps of the host and x = 1.4% Gd^{3+} concentration are shown in Fig. 4 and 5, respectively. These maps

suggest that the elemental composition present on the selected samples are distributed unevenly over the surface.

The microstructure of the host, x = 1.4 and x = 3% Gd^{3+} doped samples were examined using SEM and the results are shown in Fig. 6a, b and c, respectively. In Fig. 6a and b, it is clear that the crystallites are agglomerated and homogenously distributed. It can be observed that the crystallites with additional irregular crystallites (this is clearly illustrated on the insert of this Fig. 6b) distributed all over the surface of the agglomerated crystallites. The morphology of the sample at the higher Gd^{3+} concentration (x = 3%) shows similar kind of morphology as in Fig. 6a and b with higher degree of crystallites agglomerated together over the surface to make bigger crystallites. Therefore, the SEM results clearly indicate that the prepared nanopwders is influenced by the Gd^{3+} concentration.

3.3 TEM results

The TEM image of the host, x = 1.4 and x = 3% nanopowder are shown in Fig. 7a – c, respectively. Due to the high degree of crystallites agglomeration for the host sample shown in Fig. 7a and b, it is not an easy task to predict the accurate crystallite sizes. However, the crystallites agglomeration for the x = 1.4% (see Fig. 7b) seems to have been diminished lesser compared to the host sample, which is exactly what was observed on the SEM results in Fig. 6a and b. For the x = 3%, it can be noticed that the average crystallite sizes is around 10 nm, which agrees with the XRD results presented in Table I. The lattice fringes for the samples presented in Fig. 7a – c can clearly be observed on the zoomed version shown in Fig. 7d – e, respectively. The related SAED images confirms that the prepared nanopowders are crystalline as it was suggested by the XRD results. Furthermore, the SAED patterns indicate that the intensities of bright spots varies with Gd^{3+} doping concentration, which suggests different crystallite sizes.[34]

3.4 PL results

Fig. 8a demonstrated the excitation and emission spectra of the $MgAl_2O_4$:x% Gd^{3+} ($0 \leq x \leq 3$) series. The excitation spectra measured when monitoring the emission at 385 nm revealed that there are three excitation bands located at around 225, 275 and 335 nm. The band at 225 nm (5.51eV) is attributed to band-to-band transition and the motive being the fact that the band gap (E_g) of $MgAl_2O_4$ can range from 5.1 - 5.8 eV.[35,36] The 275 nm excitation is attributed to be due to the host defects for the un-doped sample,[23] which is surely not the case for the Gd^{3+} doped samples (only if we assume that the Gd^{3+} ground state is located at the edge of the host valence band (VB) as shown in Fig. 10) and this will be explained later in this paper. The 335 nm excitation is purely attributed to arise from the defects absorption within the host in

all samples.[23] The results also showed that when exciting the Gd^{3+} doped samples at 275 nm, there are three emission peaks located at 315, 385 and 628 nm. The intense emission peak at 385 nm is attributed to originating from the intrinsic intraband gap defects within the host material.[23] The emission band at 315 nm is related to transitions of Gd^{3+} ion corresponding to the $^6P_{7/2} \rightarrow {}^8S_{7/2}$.[37-40]. The emission at 628 nm can either be attributed to the $^6G_{7/2} \rightarrow {}^8P_{3/2}$ (Gd^{3+} transition) or second order emission of $^6P_{7/2} \rightarrow {}^8S_{7/2}$ (315 nm). Since it is not an easy task to differentiate the second order and $^6P_{7/2} \rightarrow {}^8S_{7/2}$ Gd^{3+} transition, in this study, we propose that the emission at 628 nm might only be due to the second order contribution not the $^6G_{7/2} \rightarrow {}^8P_{3/2}$ Gd^{3+} transition. The reason being the fact that the excited electrons cannot reach (taking into account the 275 nm excitation used in this study) the conduction band (CB) of the host material where the ^6G_j excited state or levels of the Gd^{3+} is found. Thus, the 628 nm ($^6G_{7/2} \rightarrow {}^8P_{3/2}$) from Gd^{3+} is therefore unreasonable and hence the 628 nm is attributed to the second order emission of $^6P_{7/2} \rightarrow {}^8S_{7/2}$ (315 nm). In order to investigate the effects of the Gd^{3+} doping into the host lattice, the normalized emission as a function of wavelength is presented in Fig. 8b. It can clearly be seen that there is a slight emission peak shift to the higher wavelength with an increase in Gd^{3+} concentration. The peak shift from 385 to 392 nm is certainly attributed to arise from the host since the emission at around 385 - 392 nm (violet) is not the characteristic of the Gd^{3+} spectroscopy.[37-40] Therefore, the results suggest that as the Gd^{3+} concentration is increased, the defects levels within the host responsible for the 385 nm is slightly modified or shifted a little bit downwards within the E_g. Thus, it is reasonable to conclude that Gd^{3+} serves as a very unique foreign candidate into the host crystal structure, which donates the observed emission located at 315 nm. This results also suggest that the Gd^{3+} is responsible to controls or slightly adjusting the violet emission originating from the host materials (385 – 392 nm). In addition to this, our group[41] have previously observed an emission at 388 - 392 nm in $MgAl_2O_4$:0.3% In^{3+} system, which were both attributed to originate from the host. Therefore, this further gives an evidence without any doubt that the violet emission in this study is due to the host material. In comparison to the Gd^{3+} doped $MgAl_2O_4$ synthesized by combustion method in 5 min reported by Singh et al. [11] we emphasize that in this results, the emission linked to the 306 nm was not observed. However, the additional emission due to the host and depending on the Gd^{3+} concentration located at 385 and 392 nm were observed and these emissions were not observed in ref.[11] It is also important to note that the excitation wavelength used in ref[11] and the current study is almost the same. It is with this concept which makes this study different and unique from the ref.[11] Firstly, this study and ref[11] results suggest that the luminescence properties of the prepared phosphor material might probably be depending on the synthesis method. Secondly, this study evidently shows how the Gd^{3+} concentration is regulating the emission from the $MgAl_2O_4$ (host).

Fig. 8c shows the emission intensity of the violet emission (located at 385 - 392 nm) as a function of the Gd^{3+} concentration. The results shows that the luminescence intensity decreases linearly with an increase in Gd^{3+} concentrations. The decrease in luminescence is attributed to the concentration quenching.[42,43] In order to determine the critical energy transfer distance (R_c)[44] between the neighboring Gd^{3+} ions, it is clear that further investigation at a range of ($0 \leq x \leq 1.2$) must be conducted urgently. Such investigation will also serves as the main drive to explore the possibilities of enhancing and optimizing the violet emission from $MgAl_2O_4$:x% Gd^{3+} nanophosphor. The zoomed version of the emission intensity from 315 nm as a function of wavelength is shown in Fig. 9a. Fig. 9b illustrates the emission intensity from 315 nm as a function of the Gd^{3+} concentration, which shows that the 1.8% Gd^{3+} is the optimum concentration for the 315 nm emission. An increase in luminescence at the lower Gd^{3+} concentration ($x < 1.8$) is attributed to the luminescence enhancement, while the decrease in luminescence at the higher Gd^{3+} concentration is attributed to the concentration quenching.[42,43] Note that the emission at 628 nm (not shown in this paper) shows similar behavior as the 315 nm emission.

The proposed excitation and emission channels on the $MgAl_2O_4$:x% Gd^{3+} ($0 \leq x \leq 3$) series is summarized in Fig. 10. The following abbreviations have been used: intrinsic defects level (DL) and electrons de-excite by non-radiative emission (indicated by the *). After the excitation at 275 nm (which can either excite the electron from the VB to the trap level (of the host) situated around 4.5 eV or the electron can be excited from the $^8S_{7/2} \rightarrow {}^6I_{5/2}$ if we assume that the ground state ($^8S_{7/2}$) of the Gd^{3+} is positioned at the edge of the VB), the excited electrons can either follow the emission from the host 385 - 392 nm or can be de-excited via Gd^{3+} cascade emission, which can lead to the 315 nm emissions.[39]

The luminescence decay curves for the prepared $MgAl_2O_4$:x% Gd^{3+} phosphor is shown in Fig. 11. All the decay time curves were obtained when exciting at 275 nm for the emission at 385 nm. The results indicate that all the prepared samples have the same afterglow decay mechanism, which could be fitted using the second order exponential decay. The calculated fast $\boldsymbol{\tau_1}$ and slow $\boldsymbol{\tau_2}$ decay times are presented in Table I for each sample.

Fig. 12 shows the Commission on Illumination (CIE) chromaticity diagram of the $MgAl_2O_4$:x% Gd^{3+} ($0 < x \leq 3$) series determined using the CIE coordinate calculator software.[45] Based on the emission spectra, the software shows the position of the coordinates in the chromaticity diagram and the expected color of the material. The (*x; y*) color coordinates are presented in Table I. The CIE results showed that all of the prepared samples exhibit violet emission located all most on the same position. Thus, the results suggest that the emission color cannot significantly be tuned by varying the Gd^{3+} concentration.

4. Conclusion

$MgAl_2O_4$:x% Gd^{3+} ($0 \leq x \leq 3\%$) powder phosphors were successfully prepared by sol-gel technique. The XRD patterns indicated that all the prepared samples consists of the cubic phase and Gd^{3+} ions were successfully incorporated into the crystal lattice of $MgAl_2O_4$ matrix. The SEM results revealed that the morphology of the samples is influenced by the Gd^{3+} concentration. The expected elements (Mg, Al, O, and Gd^{3+}) were confirmed by the EDS analysis. The TEM analysis confirmed that the prepared samples are on the nano-scales, which clearly agrees very well with the XRD results. The PL results showed that the violet emission is due to Gd^{3+} ions associated with $^6P_{7/2} \rightarrow {}^8S_{7/2}$ while the 628 nm could not be attributed to the $^6G_{7/2} \rightarrow {}^6P_{3/2}$ transitions but it was attributed to the 315 nm second order emission. Decay curves indicated that all the samples have the same afterglow decay mechanism. The CIE color coordinates show that the samples exhibit violet color emission, which were not influenced by varying the Gd^{3+} concentration.

Acknowledgements

This work is supported by the South African National Research Foundation (NRF) Thuthuka Programme (fund number: UID99266) and NRF incentive funding for rated researchers (IPRR) (Grant No: 114924).

References

1. V. Singh, M.D.M. Haque, and D-K. Kim, *Bull. Chem. Soc.* 28, 2477 (2007).
2. A.F. Dericioglu, A.R. Boccaccini, I. Dlouhy, and Y. Kagawa, *Mat. Trans.* 46, 996 (2005).
3. I. Ganesh, S. Bhattacharjee, B.P. Saha, R. Johnson, K. Rajeshwari, and R. Sengupta, *Cer. Inter.* 28, 245 (2002).
4. L. Thome, A. Gentils, J. Jagielski, F. Garrido, and T. Thome, *Vacuum* 81, 1264 (2007).
5. P.M. Ajayan, P. Redlich, and M. Ruhle, *J. Microsc.* 185, 275 (1997).
6. Z. Wang, C.L. Chang, X. Zhao, W. Qian, X. Zhang, Z. Xie, B.H. Hwang, C. Hu, J. Shen, and R. Hui, *J. Power Sour.* 190, 351 (2009).
7. I. Omkaram, B. Vengala Rao, and S. Buddhudu, *J. Alloy Compd.* 474, 565 (2009).
8. S.A. Bocanegra, S.R. de Miguel, A.A. Castro, and O.A. Scelza, *Catal. Lett.* 96, 129 (2004).
9. J. Sehested, A. Carlsson, T.V.W. Janssens, P.L. Hansen, and A.K. Datye, *J. Catal.* 197, 200 (2001).
10. S. Zhao, L. Wang, L. Yang, and Z. Wang, *Phys. B.* 405, 3200 (2010).
11. V. Singh, G. Sivaramaiah, J.L. Rao, and S.H. Kim, *J. Lumin.* 143, 162 (2013).

12. L. Omkaram, G.S.R. Raju, and S. Buddhudu, *J. Phys. Chem. Solids* 69, 2066 (2008).

13. S.P. Khatkar, S.D. Han, V.B. Taxak, D. Kumar, and R. Kumar, *J. Lumin.* 126, 597 (2007).

14. Y. Katayama, and S. Tanabe, *Mat.* 3, 2405 (2010).

15. B. Han, H. Liang, Y. Huang, Z. Gao, Y. Tao, and Q. Su, *App. Phys. B.* 104, 241 (2011).

16. C. Cao, W. Qin, J. Zhang, Y. Wanh, P. Zhu, G. Wei, G. Wang, R. Kim, and L. Wang, *Opt. Lett.* 33, 857 (2008).

17. P.P. Mokoena, I.M. Nagpure, V. Kumar, R.E. Kroon, E.J. Olivier, J.H. Neethling, H.C. Swart, and O.M. Ntwaeaborwa, *J. Phys. Chem. Solids* 75, 998 (2014).

18. M.K. Naskar, and M. Chattarjee, *J. Amer. Cer. Soc.* 88, 38 (2005).

19. C.R. Bickmore, K.F. Waldner, and D.R. Treadwell, *J. Amer. Cer. Soc.* 79, 1419 (1996).

20. C.T. Wang, L.S. Lin, and S.J. Yang, *J. Amer. Cer. Soc.* 75, 2240 (1992).

21. F. Tavangarian, and R. Emadi, *J. Alloys Comp*. 489, 600 (2010).

22. M. Zawadzki, J. Wrzyszcz, W. Strek, and D. Hreniak, *J. Alloys Compd.* 323-324, 279 (2001).

23. S.V. Motloung, F.B. Dejene, M.E. Sithole, L.F. Koao, O.M. Ntwaeborwa, H.C. Swart, and T.E. Motaung, *J. Electr. Mater.* 45, 4796 (2016).

24. B.D. Cullity and S.R. Sock, *Elements of X-ray Diffraction*, 3rd ed. (Reading: Pearson Education, 2001), pp. 402-404.

25. S.V. Motloung, F.B. Dejene, R.E, Kroon, O.M. Ntwaeaborwa, H.C. Swart, and T.E. Motaung, *Optik.* 131, 705 (2017).

26. S.V. Motloung, P. Kumari, L.F. Koao, T.E. Motaung, T.T. Hlatshwayo, and M.J. Mochane, *Mater Today Commun.* 14, 294 (2018).

27. S. Iaiche, and D. Djelloul, *J. Spectrosc.* 2015, 1 (2015).

28. P.U. Aparna, N.K. Divya, and P.P. Pradyumnan, *J. Mat. Sci. Chem. Eng.* 4, 79 (2016).

29. I. Miron, and I. Grozescu, *Optoelect. Adv. Mat.* 6, 673 (2012).

30. S. Saha, S. Das, U.K. Ghorai, N. Mazumder, B.K. Gupta, and K.K. Chattopadhyay, *Dalton Trans.* 42, 12965 (2013).

31. S.V. Motloung, F.B. Dejene, H.C. Swart, and O.M. Ntwaeaborwa, *J. Sol-Gel Sci. Technol.* 70, 422 (2014).

32. S.V. Motloung, F.B. Dejene, H.C. Swart, and O.M. Ntwaeaborwa, *Cer. Int.* 41, 6776 (2015).

33. L.F. Koao, F.B. Dejene, M. Tsega, and H.C. Swart, *Phys. B.* 480, 53 (2016).

34. B.S. Mwankemwa, M.J. Legodi, M. Mlambo, J.M. Nel, and M. Diale, *Superlattices Microstruct.* 107, 163 (2017).
35. R. Paiva, M. Carvalhaes, and A.R. Blak, *Phys. Stat. Sol. (c)* 4, 1238 (2007).
36. S.K. Sampath, D.G. Kanhere, and R. Pandey, *J. Phys. Condens. Matter.* 11, 3635 (1999).
37. J. Zhong, H. Liang, Q. Su, J. Zhou, and Y. Huang, *Appl. Phys. B.* 98, 139 (2010).
38. Q. Wang, S-Y. Ouyang, W-H. Zhang, B. Yang, Y-P. Zhang, and H-P. Xia, *Acta Metall. Sin. (Engl. Lett.)* 28, 487491 (2015).
39. P. Gupta, A.K. Bedyal, V. Kumar, Y. Khajuria, S.P. Lochab, S.S. Pitale, O.M. Ntwaeaborwa, and H.C. Swart, *Mat. Res. Bull.* 60, 401 (2014).
40. B.P. Singh, A.K. Parchur, R.S. Ningthoujam, A.A. Ansari, P. Singh, and S.B. Rai, *Dalton Trans.* 43, 4779 (2014).
41. L.T. Melato, T.E. Motaung, O.M. Ntwaeaborwa, and S.V. Motloung, *Opt. Mat.* 66, 319 (2017).
42. Q.Y. Zhang, and X.Y. Huang, *Prog. Mater. Sci.* 55, 353 (2010).
43. H. Tang, H. Berger, P.E. Schmid, F. Levy, and G. Burri, *Solid State Commun.* 87, 847 (1993).
44. G. Blasse, *J. Solid State Chem.* 62, 207 (1986).
45. http://www.mathworks.com/matlabcentral/fileexchange/29620-cie-coordinate-calculator (2012). Accessed 21.10.12.

List of figures

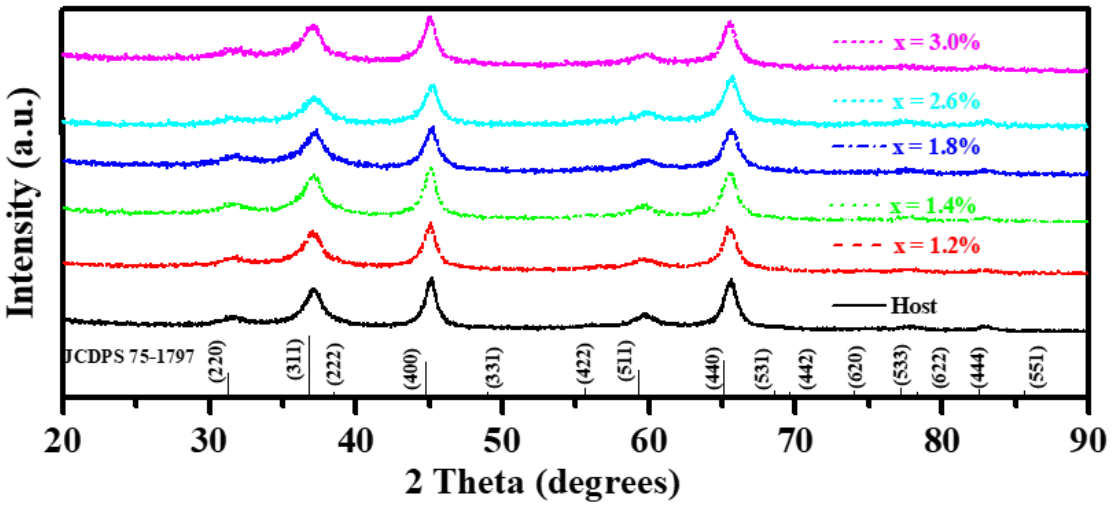

Fig. 1. The XRD pattern of the $MgAl_2O_4$:x% Gd^{3+} ($0 \leq x \leq 3$) series.

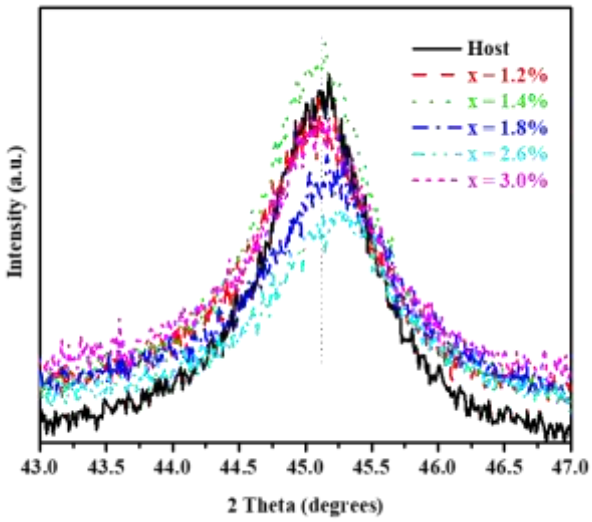

Fig. 2. The analysis of (400) diffraction peak for the $MgAl_2O_4$:x% Gd^{3+} ($0 \leq x \leq 3$) series.

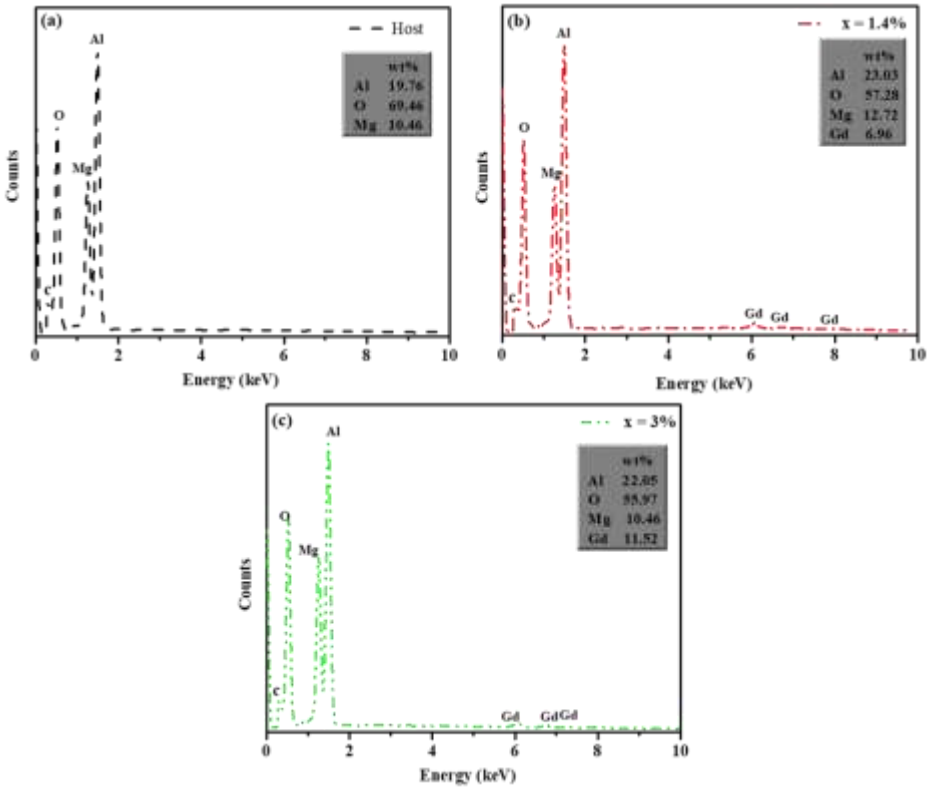

Fig. 3. The EDS spectrum for (a) host, (b) x = 1.4 and (c) x = 3%.

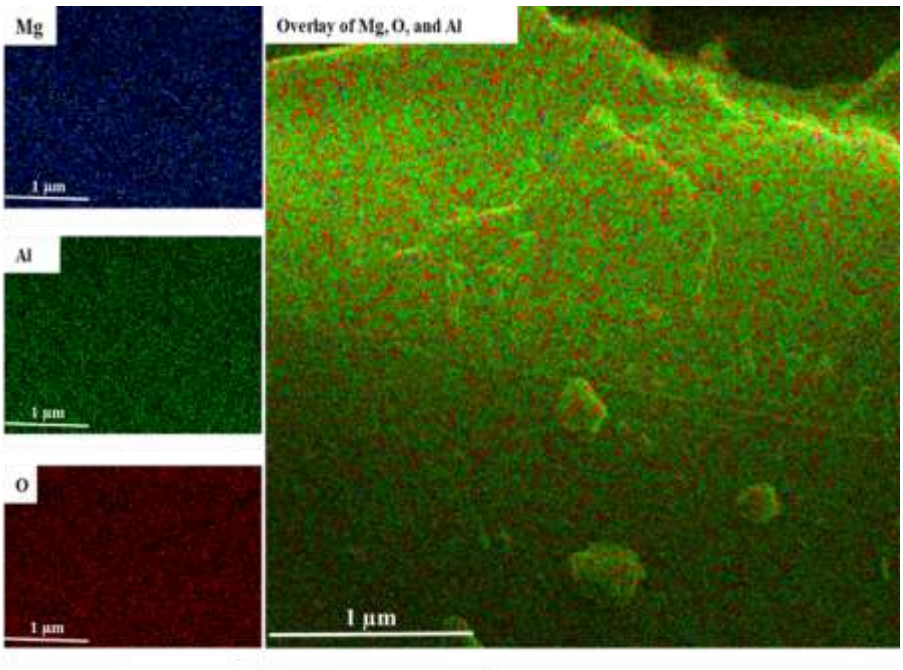

Fig. 4. The EDS map for the host ($MgAl_2O_4$).

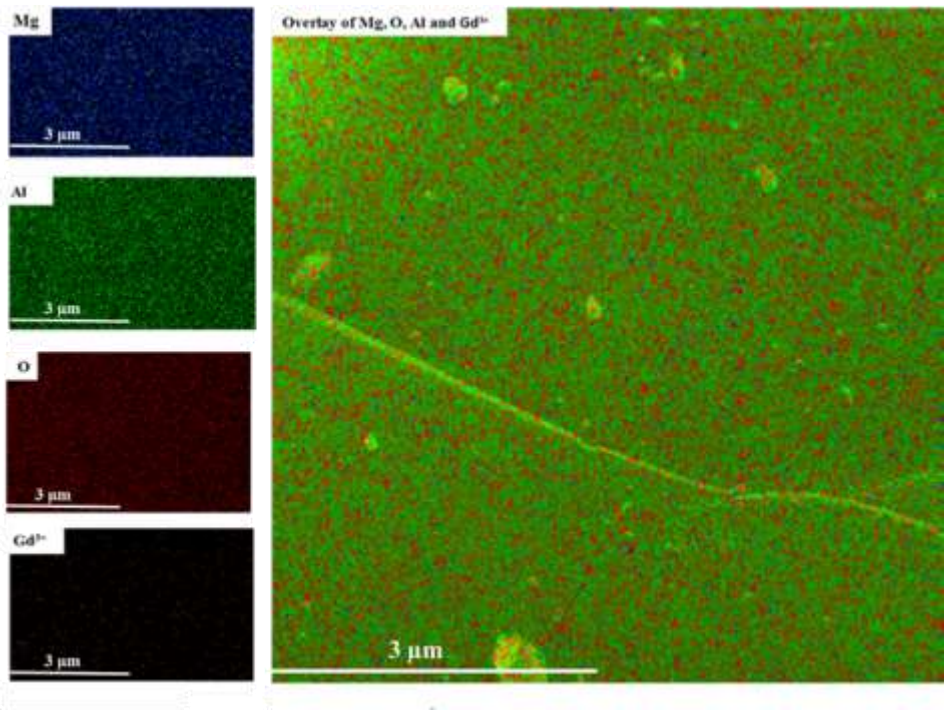

Fig. 5. The EDS mapping for the x = 1.4% Gd^{3+} doped sample.

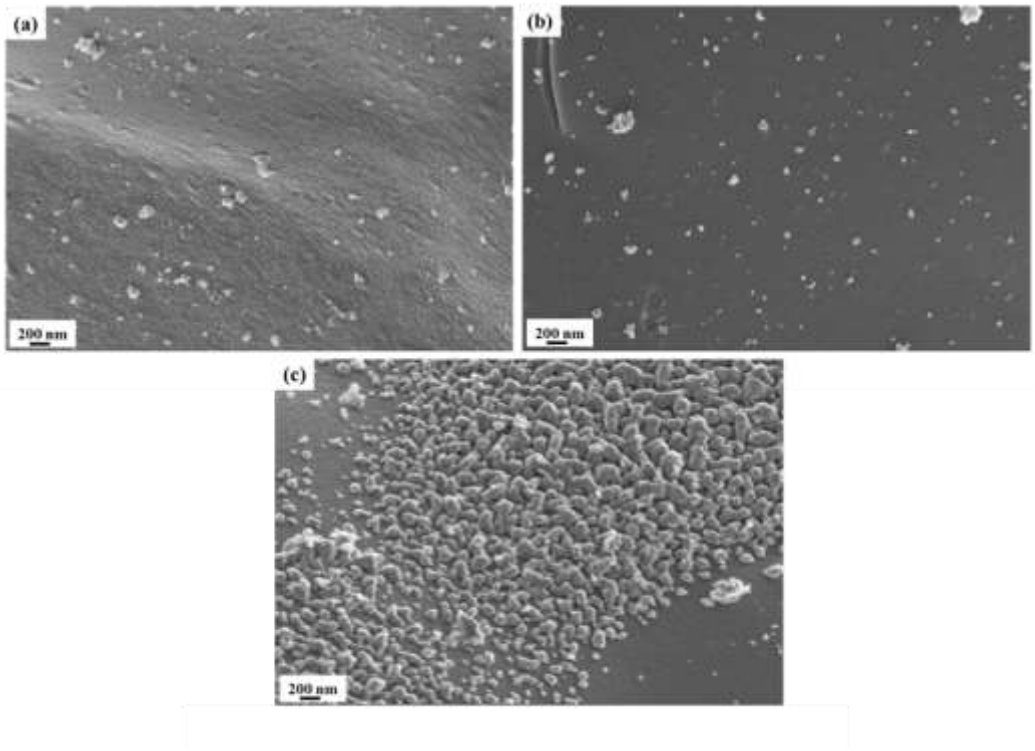

Fig. 6. SEM images of the (a) host, (b) x = 1.4 and (c) x = 3 %.

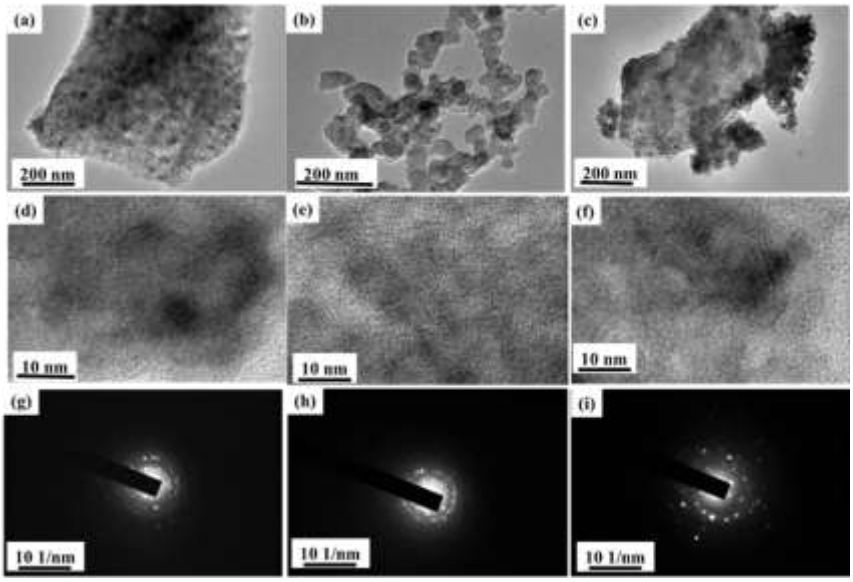

Fig. 7. TEM images of the (a) host, (b) x = 1.4, (c) x = 3 %, (c) – (f) zoomed version of the (a) – (c) images and (g) – (h) SAED images of the (a) – (c) samples, respectively.

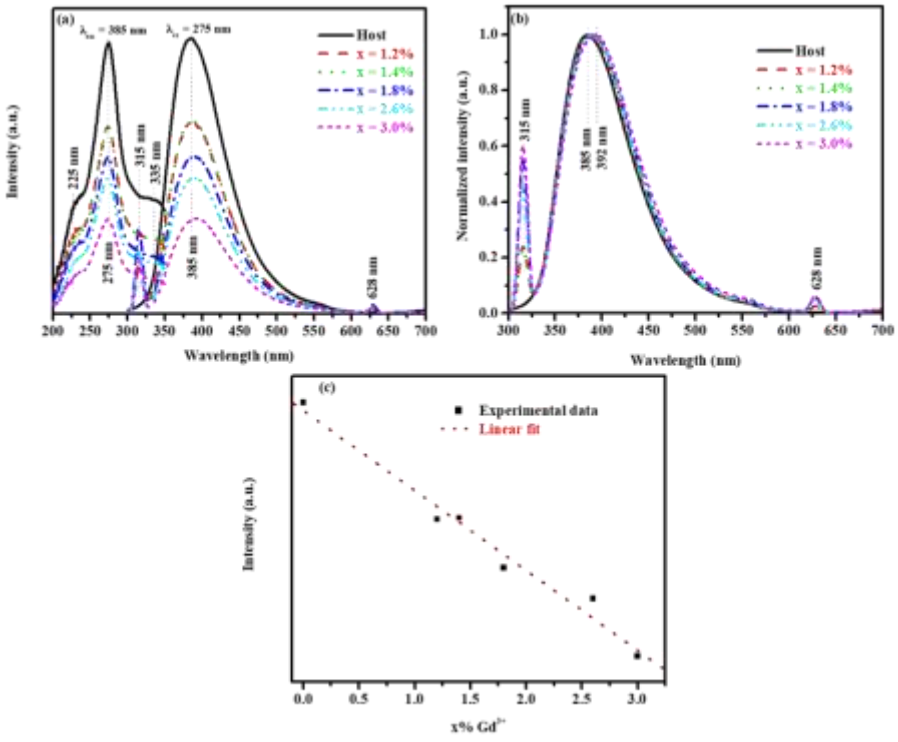

Fig. 8. (a) Excitation and emission spectra of the series $MgAl_2O_4$: x% Gd^{3+} ($0 \leq x \leq 3$) (b) normalized emission spectra of the $MgAl_2O_4$: x% $Gd^{3+}$and (c) violet emission (at 385 - 392 nm) intensity as a function of x% Gd^{3+}.

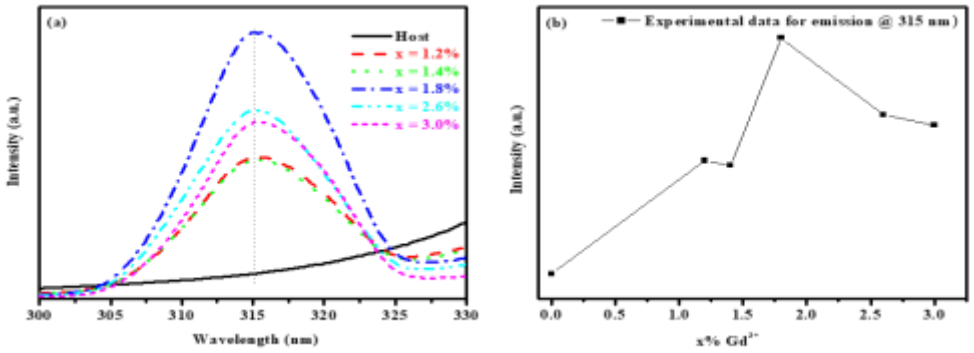

Fig. 9. (a) Emission spectra of the $MgAl_2O_4$: x% Gd^{3+} ($0 \leq x \leq 3$) series for the 315 nm and (b) x% Gd^{3+} as a function of emission intensity.

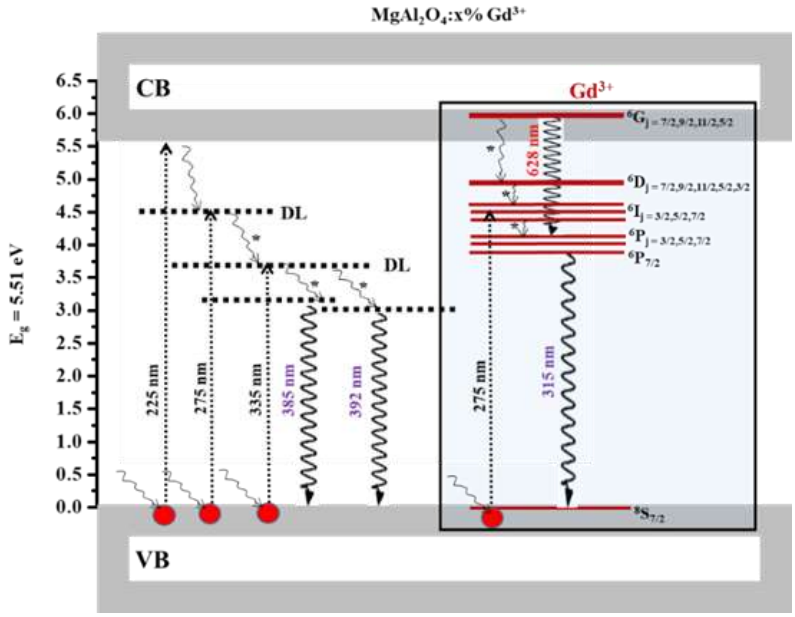

Fig. 10. The proposed excitation and emission pathways mechanism on the $MgAl_2O_4$:Gd^{3+} ($0 \leq x \leq 3$) series.

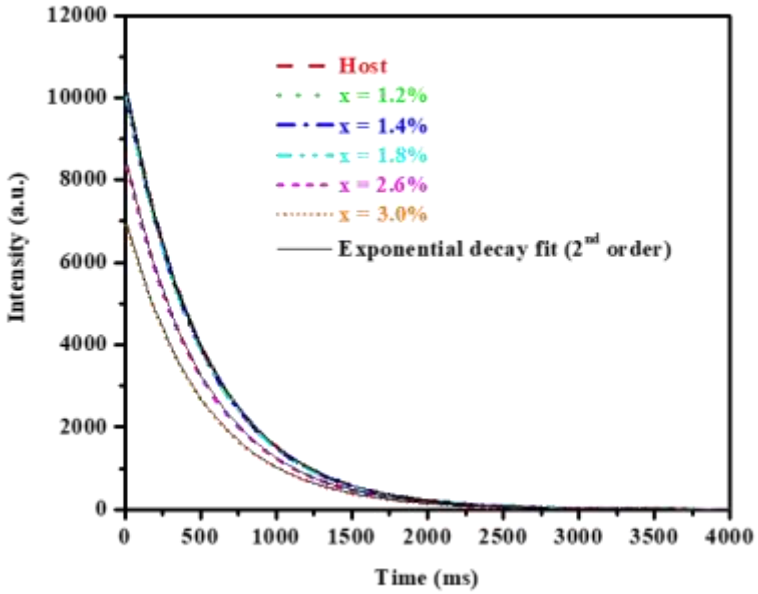

Fig. 11. The decay curves of $MgAl_2O_4$:x% Gd^{3+} ($0 \leq x \leq 3\%$) series.

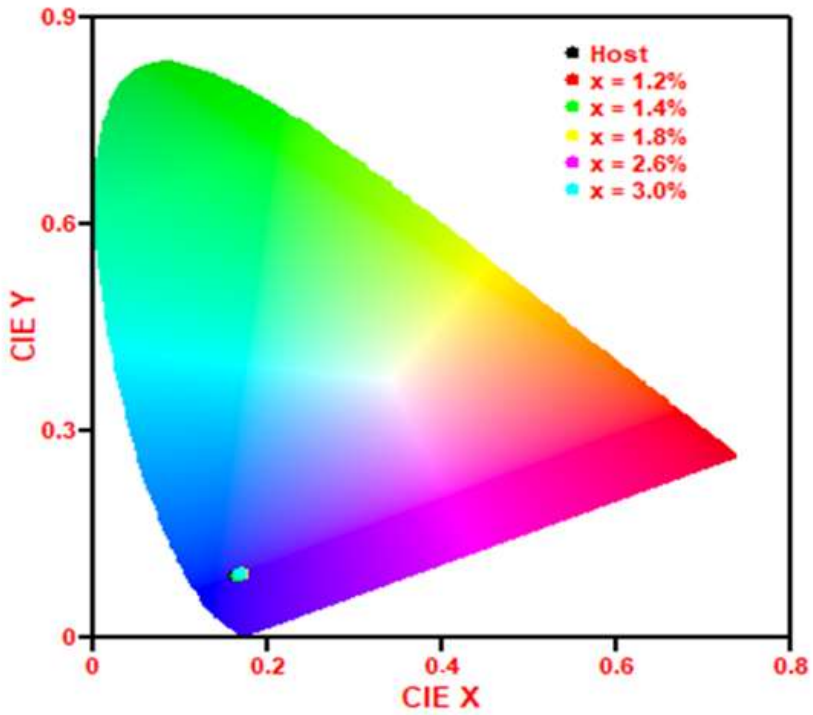

Fig. 12. CIE color of the $MgAl_2O_4$:x% Gd^{3+} ($0 \leq x \leq 3\%$) series.